Wide field-of-view imaging spectrometer using imaging fiber bundles

Xin Cheng,[1,2] Jing Wang,[1,*] Qingsheng Xue,[1] Yongfeng Hong,[1] and Shi Li[3]

[1]Changchun Institute of Optics, Fine Mechanics and Physics, Chinese Academy of Sciences, Changchun 130033, China

[2]Graduate University of Chinese Academy of Sciences, Beijing 100039, China

[3]Institute of Graphics and Image, Hangzhou Dianzi University, Hangzhou 310018, China

*Corresponding author: cleresky@vip.sina.com

Received 28 June 2011; revised 4 September 2011; accepted 4 September 2011; posted 7 September 2011 (Doc. ID 150013); published 2 December 2011

A field-of-view-folding approach is proposed to extend the field of view (FOV) of a dispersive imaging spectrometer after introducing several linear arrays of imaging fiber bundles to which to replace the slit. The fiber bundles can flexibly connect fore-optics with a spectrometer to yield an imaging fiber-optic spectrometer (IFOS). The technology of FOV segmenting and folding, which can decrease simultaneously the dimension and spectral distortion of the imaging spectrometer, is described in detail. Because of the sampling function of the fiber bundles, the IFOS is a double-sampling imaging system. We analyze the effect of fiber coupling on the modulation transfer function (MTF) and then develop a cascade MTF model to estimate the imaging performance of the IFOS. A spaceborne IFOS example is presented to describe how the method can be used. © 2011 Optical Society of America

OCIS codes: 120.3620, 110.4100, 110.4234, 060.2350.

1. Introduction

The imaging spectrometer is a well-established technique for achieving the spatial and spectral information of the target simultaneously. One of the important features of a next-generation imaging spectrometer is wide field of view (FOV), which has received less attention until recently. A wide field imaging spectrometer that explored the Earth atmosphere from low Earth orbit had an FOV as wide as 70° [1]; another one designed for coastal ocean detection had a large FOV of 36° [2]. However, the main reasons wide FOV can be obtained for them are low operation height and short focal length, as we know that, with a given format of focal plane array (FPA), short focal length usually allows an imaging spectrometer to achieve wide FOV. In general, the FOV of an imaging spectrometer is primary restricted by the format of the FPA. With a larger-sized one, a wider FOV could be obtained, just as the Maritime Hyperspectral Imager designed at the Naval Research Laboratory, which had a 4° field from 600 km altitude [3]. Consequently, increasing the size of the FPA by geometrically splicing multiple FPA components in the spatial direction will eventually increase system FOV. According to Cook's description, an ultrawide FOV imaging spectrometer based on reflective triplet form has been successfully built at Raytheon [4]. The slit format is 65 mm, and dozens of slits and FPA components were utilized to realize the wide FOV. However, with the enlargement of the FOV, the dimension and weight of the spectrometer are increased, and the spectral distortion, typically termed smile and keystone, are also increased. Wide FOV can be realized in a number of other ways including multibarrel [5,6], multispectrometer [7], and even multiple imaging spectrometers using field splicing [8]. Among them, the middle one shows an enormous potential in wide FOV application, which proposes behind relays on splitting the huge FOV in smaller portions, each of them reimaging onto a reasonable size detector

0003-6935/11/356446-06$15.00/0
© 2011 Optical Society of America

through an individual spectrometer. In this arrangement, although the distortion would be controlled readily, the volume and weight does not decrease essentially.

In general, the optomechanical configuration determines the dimension and weight of the remote sensing instrument; thus, increasing the FOV physically will induce a bulky structure, especially for the imaging spectrometer, which also generates a great spectral distortion. Here we show an FOV-folding approach that can significantly enlarge the FOV of the imaging spectrometer but still make them compact and meanwhile keep the spectral distortion in micrometer magnitude. This method uses several linear arrays of imaging fiber bundles to substitute for the slit and connect fore-optics and spectrometer flexibly. Fiber bundles working as a luminous energy transmission component reformatting for spectrometers to compose a nonimaging fiber-optic spectrometer is very well known. It also was traditionally used in medical imaging systems and remote inspection devices such as flexible endoscopes involving a confocal microscope as an image transmission component. In terms of the application in integral field spectroscopy (IFS), fiber bundles were used as a field splitting component to transform a two-dimensional geometry at the focal plane of the telescope into the one-dimensional geometry at the entrance of the spectrograph [9,10]. The goal of using fiber bundles in IFS is to record simultaneously three-dimensional information of an extended object, while the goal of our proposed technology is to extend the FOV on the cross-track direction when the imaging spectrometer works in a pushbroom scan. When used in a nonimaging system, the effect of the lattice structure of fiber bundle distribution on the spatial resolution need not be considered; however, it cannot be neglected in an imaging system. The fiber bundle is a well-known discrete sampling component, combining with the detector to make the imaging fiber-optic spectrometer (IFOS) become a double-sampling imaging system. For a complex sampling imaging system with a coupling component, the influence of fiber coupling on imaging performance must be taken into consideration. Therefore, it is necessary to calculate the modulation transfer function (MTF) for the IFOS. In Section 2, we describe the FOV-folding technique using fiber bundles; in Section 3 we analyze the effect of fiber coupling on the MTF of the imaging spectrometer, and then build a cascade MTF model to evaluate the imaging performance for the IFOS. An illustrative example is given in Section 4.

2. FOV-Folding Method Using Fiber Bundles

For imaging spectrometer work in a pushbroom scan, the slit is projected on the ground and scanned forward with the platform motion. The width of the scan in the cross-track direction is the cross-track field of view (CFOV). As for the IFOS, the slit is replaced by a linear array of imaging fiber bundles; using the characteristics of flexibility and separability, we can segment the wide CFOV of the telescope or multitelescope into several smaller sub-CFOVs at the input end on the imaging plane of the telescope(s), as shown in Fig. 1(a), and then fold and arrange them at the output end on the objective plane of the spectrometer in the orthogonal direction to the CFOV [see Fig. 1(b)]. It should be noted that the intervals between each fiber bundle must be greater than the dispersive width of the spectrometer so that the spectral images of the sub-CFOVs do not overlap with the adjacent one. All sub-CFOVs are then imaged by the common spectrometer and depend on wavelengths on a common detector [see Fig. 1(c)]. After that, all of the spectral images of the sub-CFOVs are spliced into an integer in sequence by using the technique of image stitching [see Fig. 1(d)]. To achieve the same CFOV, the novel arrangement allows a more compact structure than that of a slit imaging spectrometer because all sub-CFOVs of the telescope share a common spectrometer and a single focal plane array. Moreover, the spectral distortion would be controlled easily since all the sub-CFOVs are imaged independently.

3. MTF Evaluation for IFOS

In general the shift invariant (or isoplanatic) assumption for the sampling imaging system is no longer valid. The traditional approach defining the MTF of a sampled imaging system is to analyze the impulse response by sampling and discrete Fourier transform [11,12]. The main results involving sampling and imaging effects were not suited for the cascade system; thus, the traditional method of MTF analysis cannot clearly account for the degeneration of the MTF caused by the effect factors. In a later section we will develop an MTF model for the IFOS, from which one can clearly find the effects on the MTF from the sampling process and fiber coupling.

For the imaging spectrometer designed for Earth observation, in most cases, the spectrometers have a magnification of 1× so that the slit width is matched with the size of the detector pixel. As for

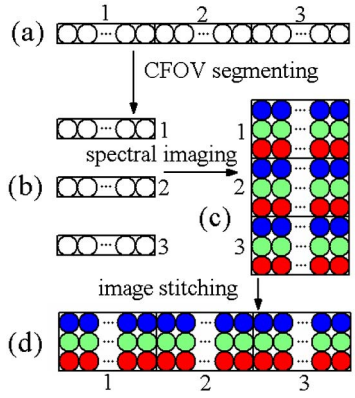

Fig. 1. (Color online) Diagrammatic sketch of distribution of fiber or spectral images (a) on the imaging plane of the telescope (at the input end of fiber bundles), (b) on the objective plane of the spectrometer (at the output end of fiber bundles), (c) on the imaging plane of the spectrometer, and (d) after image stitching.

the fiber-based imaging spectrometer, the image of fiber bundles (pseudo slit) is generally formed to cover two rows of pixels on the FPA. Therefore, in the perfect world, each fiber image for a certain wavelength would be fully matched with the corresponding 2×2 detector pixels and be sampled by them as shown in Fig. 2(a). However, the departure of the fiber image from the ideal location will be generated in the presence of the spectrometer distortion, which gives rise to a disorder to the sampling process of the detector, as shown in Fig. 2(b), and hence a degradation of imaging performance. It therefore is necessary to estimate the MTF for the IFOS. In Fig. 2(b), the vertical component of the departure is the well-known smile, and the horizontal component is termed "offset k," with the maximum value marked as "offset k_M," which are the products of the fact that the spectrometer is not distortion-free and its reduction ratio is not strictly equal to 1.

For the single fiber the assumption of a linear space invariant has been proved to be established [13] based on which MTF model is built up. For the sake of simplicity, the following analysis is limited to the one-dimensional case, and the expression can be expanded to the two-dimensional case also. In general, two MTFs are involved in the sampling process [14]: the integral MTF as a result of pixel size, $\mathrm{MTF}_{\mathrm{int}}$, and the fictitious sampling MTF caused by spatial sampling rate, $\mathrm{MTF}_{\mathrm{sam}}$. Reference [13] indicates that the aperture function of the integral surface could be regarded as the fictitious point-spread function (PSF) for a sampling component. In the case of a perfect match [see Fig. 3(a)], the entire fiber core is sampled by the corresponding 2×2 pixels; thus, the aperture function of core is the fiber PSF, and the integral MTF of sampling process is given by

$$\mathrm{MTF}(f)_{a-\mathrm{int}} = |F(f)||G(f)|, \tag{1}$$

where $F(f)$ and $G(f)$ are the Fourier transforms of the aperture function of fiber core and rectangular detector pixel, respectively. Here they are well-known functions expressed as

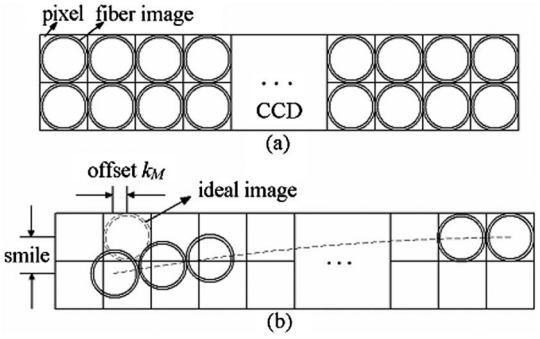

Fig. 2. Match state between the image of fiber bundle and FPA for a certain wavelength (only half the fiber bundle is drawn; the other half gives symmetrical results): (a) perfect match and (b) mismatch (for clear illustration, each square includes 2×2 sampling pixels).

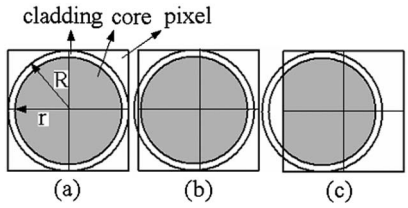

Fig. 3. Match state for a single fiber and corresponding pixels when (a) $k_M = 0$, (b) $0 < k_M \le R - r$, and (c) $k_M > R - r$.

$$F(f) = \frac{J_1(2\pi r f)}{\pi r f}, \tag{2}$$

$$G(f) = \mathrm{sinc}(Rf), \tag{3}$$

where r and R are the radius of the cross sections of the fiber core and fiber, respectively, with pixel pitch equal to R, and J_1 is the Bessel function of the first kind and of the first order. Combining Eqs. (1)–(3), we obtain the integral MTF of a perfect match,

$$\mathrm{MTF}(f)_{a-\mathrm{int}} = \frac{J_1(2\pi r f)}{\pi r f}\mathrm{sinc}(Rf). \tag{4}$$

In the case of a mismatch shown in Figs. 3(b) and 3(c), according to the theory about misalignment in fiber bundles, the average MTF model of the sampling process of a detector is given by [15]

$$\mathrm{MTF}(f)_{m-\mathrm{int}} = |F(f)||G^*(f)||P(f)|, \tag{5}$$

where $P(f)$ is the Fourier transform of distribution function of stochastic departures from the match. Since the offset k and the smile described in Fig. 2(b) are far less than fiber bundle width, the offset k_i of the ith couple of fiber and corresponding detector pixel can be regarded as uniform distribution from zero to the maximum value k_M and described by

$$p(k_i) = \begin{cases} 1/k_M, & 0 \le k_i \le k_M, \\ 0, & \text{elsewhere.} \end{cases} \tag{6}$$

Equation (6) can be expressed in another form like this:

$$p(k_i) = \frac{1}{k_M}\mathrm{rect}\left(\frac{k_i - k_M/2}{k_M}\right). \tag{7}$$

Thus, the Fourier transform of $p(k_i)$ is

$$|P(f)| = \mathrm{sinc}(k_M f), \tag{8}$$

with neglecting the parameter for the right term. Combining Eqs. (2), (3), (5), and (8), we determine the average MTF of the sampling process to be

$$\mathrm{MTF}(f)_{m-\mathrm{int}} = \frac{J_1(2\pi r f)}{\pi r f}\mathrm{sinc}(Rf)\mathrm{sinc}(k_M f). \tag{9}$$

It is to be noted that Eq. (9) accounts for rough evaluation when the setoff k_M is greater than fiber

cladding thickness. There are some details that must be considered. In the case of mismatch but with the offset k_M less than fiber cladding thickness, as shown in Fig. 3(b), the offset just introduces a phase factor after the Fourier transform, which does not contribute to MTF, and the entire core is still sampled by the corresponding pixels; thereby the MTF is the same as that of perfect match and expressed by Eq. (4). However, for the case of the offset k_M greater than fiber cladding thickness, as shown in Fig. 3(c), the accurate MTF expression,

$$\mathrm{MTF}(f)_{m-\mathrm{int}} = \frac{J_1(2\pi rf)}{\pi rf}\mathrm{sinc}(Rf)\mathrm{sinc}[(k_M - R + r)f], \tag{10}$$

should be used to replace Eq. (9). The third term of the right polynomial in Eq. (10) can be regarded as the mismatch MTF, while the product of other two terms represents the integral MTF of perfect match. So the average integral MTF is expressed as Eq. (4) when the entire fiber core is sampled by the corresponding pixels and as Eq. (10) when the fiber core is partially sampled. For fiber bundles and detector, both are sampling components and have their own sampling MTFs, which are well known and respectively given by the sinc formulas:

$$\mathrm{MTF}_{f-\mathrm{sam}} = \mathrm{sinc}(2Rf), \tag{11}$$

$$\mathrm{MTF}_{d-\mathrm{sam}} = \mathrm{sinc}(Rf). \tag{12}$$

Therefore, combining the Eqs. (4), (11), and (12), when the maximum offset k_M is less than the fiber cladding thickness, the system MTF of the IFOS can be expressed:

$$\mathrm{MTF}(f)_{a-\mathrm{sys}} = \frac{J_1(2\pi rf)}{\pi rf}\mathrm{sinc}(2Rf)\mathrm{sinc}^2(Rf), \tag{13}$$

and when the maximum offset k_M is greater than the fiber cladding thickness, it is expressed by

$$\mathrm{MTF}(f)_{m-\mathrm{sys}} = \frac{J_1(2\pi rf)}{\pi rf}\mathrm{sinc}(2Rf)\mathrm{sinc}^2(Rf)\mathrm{sinc}[(k_M - R + r)f]. \tag{14}$$

Compared with the MTF of the slit imaging spectrometer, this model has three additional terms: the integral, the sampling MTF of fiber core, and the mismatch MTF; the product of them can be regarded as coupling MTF owing to the introduction of fiber bundles.

4. Example of the Design

The following example is intended to illustrate the application of the CFOV-folding method using fiber bundles. It is a spaceborne IFOS that operates on a spectral range of 420–1000 nm with four fiber bundles replacing the slit and providing a CFOV of 11.42° for the focal length of 360 mm. The fiber bundles segment the 72 mm linear field of the Wetherell three-mirror anastigmat (TMA) telescope into four equal portions a, b, c, and d in 18 mm, as shown in Fig. 4. They are folded and arranged at the output end in the same interval along the orthogonal direction to that of an array of fiber bundles. The spectrometer reimages the images transmitted from telescope through the fiber bundles and disperses them on the FPA depending on wavelengths (A, B, C, and D in Fig. 4 are the spectral images of a, b, c, and d, respectively). Both at the input end and the output end, the linear array of the fiber bundle is fixed in V-shaped grooves (see Fig. 5) on the imaging plane of the telescope and the objective plane of spectrometer, respectively. Utilizing this arrangement, we can control the cumulative width error of the fiber bundle from the fabrication process.

The telescope in this IFOS has two functions: it forms the images of the ground strip scene on the entrance surface of the fiber bundles and then couples them into fiber bundles. Because of the circle aperture of the fiber sampling, $(1 - \mathrm{pi} \times r^2/(4 \times R^2)) \times 100\%$ of the available light is lost compared with the slit spectrometer; however, this is not a fatal drawback for a prism spectrometer. The spectrometer is an Offner type, with four Féry prisms located on the two arms symmetrically. It has a small spectral distortion similar to that of an Offner grating spectrometer and a good linearity of dispersion after the introduction of two other flint prisms [16]. Both the maximum smile and keystone of the designed IFOS are controlled less than 2 μm in CODE V, and the nonlinearity of dispersion is less

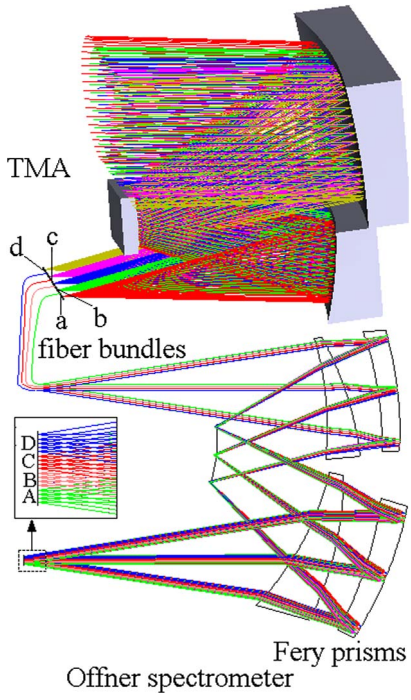

Fig. 4. (Color online) Sketch of the layout of the spaceborne IFOS.

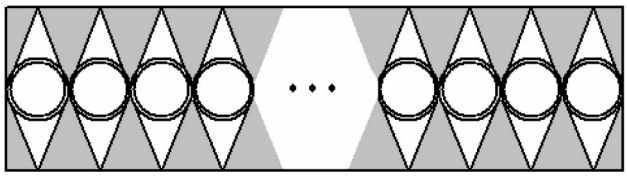

Fig. 5. Cross section of the V-shaped grooves.

than 0.15. To show that the compact structure and low spectral distortion can be obtained simultaneously for our designed FOV-folding prism spectrometer, we compare it under the same conditions with the classical Offner grating spectrometer, which is well known for a compact system design and lack of distortion. Because the system size, to a large extent, influences the image quality and spectral distortion, all of these factors are used for comparison, and the results are listed in Table 1. Here the image quality is measured in micrometers of RMS wavefront error (WFE) including average WFE and maximum WFE, and the spectral distortion including the smile and keystone are measured in micrometers. The slit format in the Offner grating spectrometer is 72 mm; some decenters are added to optimization to achieve better image quality. The designed FOV-folding spectrometer has overwhelming advantages over the designed volume, which is about one fifth of the slit one. Meanwhile, it has better image, less smile, and almost equal keystone relative to the slit one. In addition, the flexible fiber bundles permit the telescope and spectrometer to be in random arrangement and to be more compact.

To show the imaging performance of the designed IFOS and the effect of the fiber coupling on the MTF, we take the example of $R = 9\,\mu$m and $r = 8\,\mu$m and plot the system MTF without consideration of the MTF of telescope and spectrometer and then compare them with that of the slit imaging spectrometer. The maximum offset k_M described in Section 3 for fiber bundles a, b, c, and d versus three typical wavelengths are listed in Table 2, which shows that the fiber bundles have almost equal k_M at those wavelengths. Take fiber c as the example and plot MTF curves for the wavelength of 600 nm by substituting the k_M values listed in Table 2 into Eq. (14); those curves are depicted in Fig. 6. The solid squares represent the MTF of mismatch expressed by $\mathrm{sinc}[(k_M - R + r)f]$, the solid curve represents the MTF of the slit imaging spectrometer, the solid circles represent the coupling MTF of the fiber bundles, and the solid triangles represent the system MTF. It can be seen that, compared to the slit one, the system MTF is degraded by about 0.5 due to the coupling effect of the fiber bundles at the Nyquist frequency but is still acceptable.

Table 1. Parameters Comparison between the Designed FOV-Folding Spectrometer and the Classical Offner Grating Spectrometer

	FOV-Folding Prism Spectrometer	Offner Grating Spectrometer
Slit format (mm)	18×4	72
Size (mm)	$290 \times 225 \times 120$	$520 \times 340 \times 230$
Average RMS WFE (μm)	0.136	0.193
Maximum RMS WFE (μm)	0.176	0.246
Maximum smile (μm)	1.9	5.6
Maximum keystone (μm)	1.5	1.3

Table 2. Maximum Offset k_M for Fiber Bundles at Central and Marginal Wavelengths in μm

	420 nm	600 nm	1000 nm
Fiber a	11.1	11.9	12.1
Fiber b	11.2	12.0	12.3
Fiber c	11.4	12.1	12.4
Fiber d	11.5	12.3	12.6

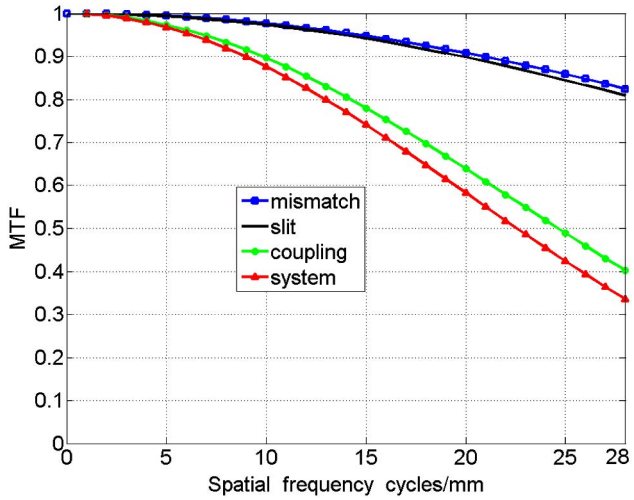

Fig. 6. (Color online) MTF curves of the slit spectrometer and the designed IFOS when the values of R and r are 9 μm and 8 μm, respectively.

5. Conclusions

We present a method of FOV enlargement for the dispersive imaging spectrometer by substituting the slit with a linear array of imaging fiber bundles. Utilizing the flexibility and separability of fiber bundles, we split the wide FOV of the telescope into several small units and then fold and arrange them on the objective plane of the spectrometer with some intervals separated between them. The images transferred from the telescope through fiber bundles are reimaged on a common detector by the spectrometer. This approach can simultaneously decrease the volume of the imaging spectrometer and the spectral distortion due to wide FOV design at the cost of MTF degradation caused by a couple function of the fiber bundles. The IFOS is a multisampling imaging system, and a cascade MTF model is developed to estimate the imaging performance. An example of a spaceborne IFOS is designed to illustrate the use of the FOV folding, and MTF curves were plotted for it, which indicates that the wide FOV and compact

structure can be obtained simultaneously at the sacrifice of partial MTF value.

This work was supported by the National Program on Key Basic Research Project (973 Program) of China under 2009CB7240020603B.

References

1. R. E. Haring, F. Williams, G. Vanstone, and G. Putnam, "WFIS: a wide field-of-view imaging spectrometer," Proc. SPIE **3759**, 305–314 (1999).
2. P. Mouroulis, R. O. Green, and D. W. Wilson, "Optical design of a coastal ocean imaging spectrometer," Opt. Express **16**, 9087–9096 (2008).
3. R. Lucke and J. Fisher, "The Schmidt–Dyson: a fast space-borne wide-field hyperspectral imager," Proc. SPIE **7812**, 78120M (2010).
4. L. G. Cook and J. F. Silny, "Imaging spectrometer trade studies: a detailed comparison of the Offner–Chrisp and reflective triplet optical design forms," Proc. SPIE **7813**, 78130F (2010).
5. J. S. Pazder, M. Fletcher, and C. Morbey, "The optical design of the wide field optical spectrograph for the thirty meter telescope," Proc. SPIE **6269**, 626932 (2006).
6. E. E. Sabatke, J. H. Burge, and P. Hinz, "Optical design of interferometric telescopes with wide fields of view," Appl. Opt. **45**, 8026–8035 (2006).
7. D. Magrin, R. Ragazzoni, G. Gentile, M. Dima, and J. Farinato, "Optical design of a highly segmented wide field spectrograph," Proc. SPIE **7428**, 7428U (2009).
8. P. Hu, Q. Lu, R. Shu, and J. Wang, "An airborne pushbroom hyperspectral imager with wide field of view," Chin. Opt. Lett. **3**, 689–691 (2005).
9. C. Vanderriest, "Integral field spectroscopy with optical fibres," in *3D Optical Spectroscopic Methods in Astronomy*, G. Comte and M. Marcelin, eds., Vol. 71 of ASP Conference Series, 209–218, (Astronomical Society of the Pacific, 1995).
10. I. R. Parry, "Optical fibres for integral field spectroscopy," New Astron. Rev. **50**, 301–304 (2006).
11. W. Wittenstein, J. C. Fontanella, A. R. Newbery, and J. Baars, "The definition of the OTF and the measurement of aliasing for sampled imaging system," Opt. Acta **29**, 41–50 (1982).
12. S. K. Park, R. A. Schowengerdt, and M. A. Kaczynski, "Modulation-transfer-function analysis for sampled image system," Appl. Opt. **23**, 2572–2582 (1984).
13. R. Drougard, "Optical transfer properties of fiber bundles," J. Opt. Soc. Am. **54**, 907–914 (1964).
14. K. M. Hock, "Effect of oversampling in pixel arrays," Opt. Eng. **34**, 1281–1288 (1995).
15. M. E. Marhic, S. E. Schacham, and M. Epstein, "Misalignment in imaging multifibers," Appl. Opt. **17**, 3503–3506 (1978).
16. S. Kaiser, B. Sang, J. Schubert, S. Hofer, and T. Stuffler, "Compact prism spectrometer of pushbroom type for hyperspectral imaging," Proc. SPIE **7100**, 710014 (2008).